Construction and Building Materials 127 (2016) 518–526

Contents lists available at ScienceDirect

Construction and Building Materials

journal homepage: www.elsevier.com/locate/conbuildmat

# Bond position function between corroded reinforcement and recycled aggregate concrete using beam tests

Haifeng Yang [a,b,*], Zhiheng Deng [a,b], Jason M. Ingham [c]

[a] College of Civil Engineering and Architecture, Guangxi University, 100 University Road, Nanning, Guangxi 530004, China
[b] Key Laboratory of Disaster Prevention and Engineering Safety of Guangxi, Nanning 530004, China
[c] Department of Civil and Environmental Engineering, University of Auckland, Private Bag 92019, Auckland, New Zealand

## HIGHLIGHTS

- The bond rigidity linearly decreases in the middle of the anchorage length.
- Increasing the RCA substitution rate had little effect on the bond position curves.
- The bond rigidity becomes more uniform as crack widths increase.
- The bond position function between corroded rebar and RAC is suggested.

## ARTICLE INFO

*Article history:*
Received 11 May 2016
Received in revised form 3 October 2016
Accepted 4 October 2016
Available online 13 October 2016

*Keywords:*
Recycled aggregate
Beam test
Bond strength
Bond position function
Corrosion crack width

## ABSTRACT

Twelve beam tests were carried out in order to investigate the bond strength and bond position function between corroded rebar and recycled aggregate concrete (RAC), with the electrochemical method adopted to accelerate steel corrosion. Three recycled coarse aggregate (RCA) replacement percentages (i.e., 0%, 50% and 100%) and 4 expected corrosion crack widths of RAC (i.e., 0 mm, 0.05 mm, 0.3 mm, and 0.6 mm) were considered. Test data was used to calculate the bond stress along the anchorage length, and the influence of both RCA replacement percentages and the corrosion cracking widths on the bond strength and bond position function between the RAC and rebar. The bond position functions for different corrosion levels of reinforced RAC were also established. The results indicated that the ultimate bond strength of reinforced RAC beams decreased overall with an increase of the RCA replacement percentage and corrosion crack width, but that the rate of decline reduced with an increase of RCA and corrosion level. The bond position curve of the reinforced RAC beams was similar to that of natural aggregate concrete (NAC) beams subjected to bending and shear stresses before and after steel corrosion, with a sharp increase of the relative bond stiffness at both anchorage ends, and an almost linear decrease of relative bond stiffness in the range of 0.15–0.85 times the anchorage length. Increasing the RCA substitution rate had little effect on the bond position curves, and the bond distribution became more uniform as the crack widths increased.



## 1. Introduction

The Chinese Academy of Building Research [1] has reported that since 2011 there has been 0.46 billion square meters of construction demolished annually in China, with the service life of most of these buildings being less than 40 years. Poor quality and weak maintenance were responsible for 19% of this construction demolition, with social and economic factors such as business interests and architectural planning problems being the primary reasons for most of the demolition. Addressing this large amount of construction waste has become a significant issue for the Chinese Ministry of Construction.

The process of crushing and then using demolished waste concrete as recycled aggregate to replace part or all of the natural aggregate in new concrete construction is considered internationally to be an important breakthrough in the sustainable development of the construction industry [2,3]. Unfortunately, the current rate of construction waste reuse in China remains low, with the use of recycled aggregates primarily limited to low-value applications such as backfill for roadbeds, or partition walls

* Corresponding author at: College of Civil Engineering and Architecture, Guangxi University, 100 University Road, Nanning, Guangxi 530004, China.
*E-mail address:* yhfgxu@aliyun.com (H. Yang).

http://dx.doi.org/10.1016/j.conbuildmat.2016.10.008
0950-0618/

in construction. Consequently, with the progress of research related to concrete containing recycled aggregate [4–6], higher-value outlets for construction waste are being sought by researchers. Experimental studies have been conducted on the possible incorporation of recycled aggregates in beams [6–9], columns [10–12], and other structural members [5,13–15], with the reuse of recycled aggregates in structural applications having been found to be technical feasible. However, adequate bond performance between steel reinforcing bars and concrete is a basic prerequisite for the two materials to work compositely, and therefore it is necessary to study the bond properties of reinforced recycled aggregate concrete before RAC can be reliably used in structural members.

The bond behavior of reinforced RAC has been previously investigated. Xiao and Falkner [16] undertook 36 pull out tests using concrete blocks with no stirrups, with results demonstrating that the bond strength between RAC and deformed reinforcement has no obvious relation with the RCA replacement percentage. The same test method was adopted by Guerra et al. [17] and by Prince and Singh [18] to investigate the effect of RCA replacement on bond strength. Butler et al. [19] and Fathifazle et al. [20] used beam-end specimens based on ASTM A944-10 [21], considering different mixture proportions of RAC. In summary, a common feature of all the aforementioned studies is that the bond stress distribution was assumed uniform over the anchorage length. In contrast, structural members are typically subjected to complex stresses, such as combined bending-shear stresses for beams, and the bond stress distribution has been experimental proven to vary along the anchorage length [22], such that the assumption of a uniformly distributed bond stress is inappropriate.

Reinforcement corrosion is a common phenomenon in China [23], with reinforcement corrosion having occurred in many buildings and bridges within their 40 year service period. The following reasons are responsible for the above phenomenon [23–25]: (1) Chlorine ion corrosion caused by a marine environment or the use of deicing salts in frigid zones; (2) Atmospheric corrosion such as acid rain and greenhouse effects caused by environmental pollution, coupled with complicated climate environments resulting in freezing and thawing; and (3) Poor construction quality control such as the use of low grade concrete and insufficient cover thickness, that has resulted in accelerated reinforcement corrosion. For those concrete structures located in an aggressive environment, steel reinforcement has corroded because of the permeation of $CO_2$, $SO_2$ and chloride ions.

It is well-known that the largest durability problem in concrete structures is caused by steel corrosion and the expansion of corrosion products, not only resulting in loss of cross section, but also causing a deterioration of bond strength due to cover splitting [26–29]. Many studies have focused on the bond deterioration properties between reinforcement and NAC, but few studies have been conducted to investigate the bond behavior of reinforced RAC including the influence of steel corrosion. Zhao et al. [30] observed the bond degradation and bond stress distribution curves between different corrosion levels of reinforcement and normal/recycled concrete using pull-out tests, with the results indicating that the middle of the specimens exhibited the highest bond rigidity. However, the effect of RCA substitution and steel corrosion level on the relative bond rigidity could not be established based on their results.

The goal of the study reported here was to investigate the bond strength and bond position function between corroded steel reinforcement and RAC using beam tests. The research was conducted considering 3 RCA replacement percentages (i.e., 0%, 50% and 100%) and 4 expected corrosion crack widths of RAC (i.e., 0 mm, 0.05 mm, 0.3 mm and 0.6 mm).

## 2. Experimental program

### 2.1. Raw material and mix ratios

Demolished old concrete pavement slabs in the urban area of Nanning, China were crushed and then sieved to obtain 5–30 mm coarse recycled aggregate, while natural coarse aggregate (NCA) was bought from a local commercial aggregate plant. The typical physical properties of the two coarse aggregate types used in the study are listed in Table 1. According to the Chinese code "Recycled Coarse Aggregate for Concrete" (GB/T 25177-2010) [31] RCA can be classified into three levels dependent on absorption characteristics, and because the absorption of the RCA used in this study was 5.96% the RCA corresponded to the third level (<8%) of GB/T 25177-2010. In addition, the RCA was intentionally not washed in order to investigate the influence of untreated RCA on the bond strength between RAC and steel reinforcement. Normal Portland cement type 42.5 compliant with the Chinese standard GB 175-2007 [32] was used for the test specimens and medium-sized natural sand was utilized as fine aggregate in the mixture. Ribbed rebar type HRB400 with a diameter of 20 mm was used as longitudinal reinforcement in the test beams, having a yield strength and elastic modulus of 358.3 MPa and $2.02 \times 10^5$ MPa respectively. Stirrup reinforcement was plain steel type HPB 300 having a diameter of 8 mm.

The mix ratios of the ordinary concrete are shown in Table 2. Three replacement percentages (R = 0%, 50%, 100%) were considered in the experimental work, and cubic specimens with sides of 150 mm were cast to confirm the compressive strength of the mixed concrete. The tested 28-day compressive strengths of RC1, RC2, and RC3 were 39.7 MPa, 40.6 MPa, and 32.0 MPa respectively. It can be observed that the concrete compressive strength with 50% replacement rate of RCA (Mix RC2) was almost the same as that of the NAC, but decreased by 19.4% when the replacement percentage was 100% (Mix RC3). This observation was attributed to the actual w/c ratio having been reduced because of the high water absorption of RCA, and the effect that a lower w/c ratio has on elevating the compressive strength. There was significant initial microcracking in the RCA, attributed to the weakness of the interface transition zone [33], resulting in the compressive strength of the RAC being lower than for NAC. These observations suggest that the compressive strength when using unwashed recycled aggregates is influenced by the compound effect of an increase due to lower actual w/c ratio and a decrease due to the reduced capacity of the interface zone of RAC, with the lower w/c ratio being the dominant contributor to strength loss when R = 50%, whereas the reduced capacity of the interface zone is the primary effect when R = 100%.

### 2.2. Beam specimens

Four groups of beams (a total of 12 beams) with a cross sectional area of 150 mm × 250 mm were designed, corresponding to 4 expected corrosion crack widths of RAC (0 mm, 0.1 mm, 0.3 mm and 0.6 mm). As shown in Fig. 1, the test beams were composed of 2 symmetrical half-beams connected by a longitudinal rebar in the lower region of the beam and by a hinge joint at the top made of a I10 steel section. The length of the rebar embedment for each half-beam was 200 mm, with PVC pipes used to de-bond the remaining bar length at both ends. Only the bonded zone was designed to be corroded, with the two measures adopted to avoid corrosion of the bar ends and stirrups in the subsequent electric accelerated corrosion test being: (1) All stirrups and the debonded length of longitudinal rebar were coated with epoxy resin; and (2) 10 mm spacing was provided between the longitudinal rebar and the stirrups as an additional assurance to prevent a short-circuit of the rebar.

**Table 1**
Physical properties of coarse aggregates.

| Aggregate type | Gradation (mm) | Observed Density (kg/m$^3$) | Bulk density (kg/m$^3$) | Water Absorption (%) | Crushed index (%) |
|---|---|---|---|---|---|
| RCA | 5–30 | 2430 | 1260 | 5.96 | 19.5 |
| NCA | 5–30 | 2760 | 1429 | 1.35 | 13 |

**Table 2**
Mix ratios.

| No. | w/c | R (%) | Ingredients (kg/m$^3$) | | | | |
|---|---|---|---|---|---|---|---|
| | | | RA | NA | C | S | W |
| RC1 | 0.5 | 0 | 0 | 1150 | 420 | 750 | 210 |
| RC2 | 0.5 | 50 | 575 | 575 | 420 | 750 | 210 |
| RC3 | 0.5 | 100 | 1150 | 0 | 420 | 750 | 210 |

w/c is water/cement ratio; R is replacement percentage, C is cement, S is sand, W is mixing water.

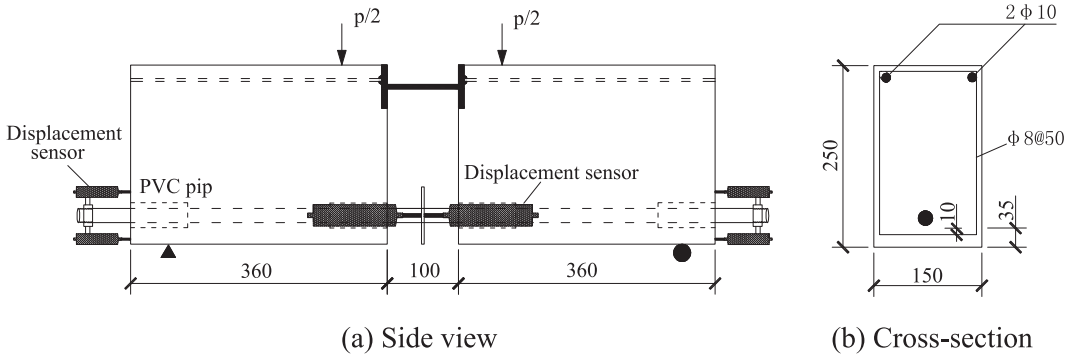


**Fig. 1.** Details of beam specimen (dimensions in mm).

To obtain the actual bond distribution in the reinforced RAC beam, the longitudinal reinforcement was processed as follows: (1) The bars were cut in half along their longitudinal axis using a computer controlled machine, with a slot cut into each half rebar having a size of 5 mm wide × 2.5 mm deep, as shown in Fig. 2(a); and (2) Strain gauges measuring 1 mm × 1 mm were pre-attached at different locations within the slot, and 0.5 mm diameter headset wires were connected to each gauge Fig. 2(b).

### 2.3. Steel corrosion test

The electrochemical method was adopted to accelerate rebar corrosion and 5% NaCl solution was used to mix the RAC in order to disseminate uniform chloride seeds in the concrete specimens, instead of using pure water. After 28 days standard curing all beams were first immersed in 5% NaCl solution for 3 days to ensure enough free chlorine ions and water in the RAC matrix for use in the subsequent corrosion test. The NaCl solution level was designed to be lower than the rebar position during the process of electrochemical corrosion in order to avoid a short circuit (Fig. 3). Next, the longitudinal beam reinforcement was connected in series and attached to the regulator anode, while the copper plate was placed into the NaCl solution and connected to the regulator cathode. Finally, a constant current (0.12 A) controlled by a DC power source was applied between the longitudinal bars and the copper plate. Because the reinforcement corrosion rate could not be directly measured due to the limited range and precision of the electronic scale, Faraday's law and expected crack widths [34,35] were adopted as methods to estimate and control the corrosion rate, as shown as Eq. (1).

$$\eta = \frac{\Delta w}{m} = \frac{MIt}{2mNe} \tag{1}$$

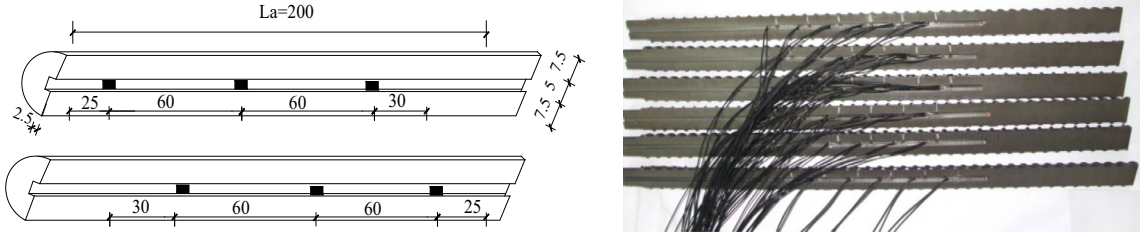


**Fig. 2.** Rebar processing.

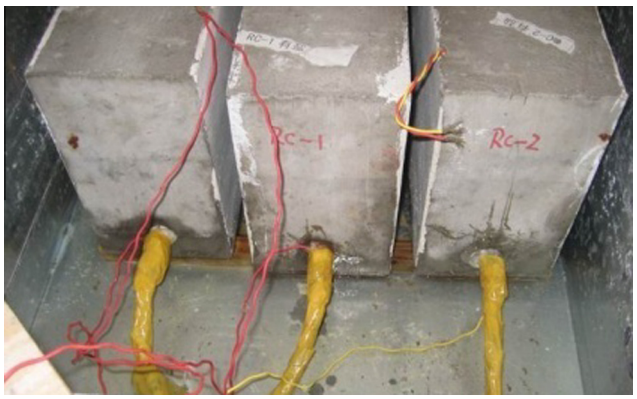


**Fig. 3.** Electrochemical process.


**Fig. 4.** Setup for loading.

where $\eta$ is corrosion rate; M is the molar mass of the rebar (56 g/mol); $I$ (A) is the constant current (0.12 A); $t(s)$; N is the Avogadro Constant ($6.02 \times 10^{23}$ mol$^{-1}$); $m$ is the mass of the anchored rebar (un-corroded); and $e$ is the electron charge ($1.6 \times 10^{-19}$ °C).

### 2.4. Loading test

Fig. 4 shows the setup for loading, with the loading jack and reaction frame being configured to apply two concentrated loads with simply supported boundary conditions. Loading was controlled by a pressure sensor and was applied incrementally, with each load grading lasted about 5 min. Slip between the rebar and concrete at both ends of the each beam specimen was measured using displacement sensors, and strain data from the longitudinal rebar were recorded using a static strain acquisition instrument synchronized to the applied loading.

## 3. Test results and discussion

### 3.1. Failure pattern

The maximum crack width at the base of the beam was measured after each corrosion test, with corrosion-induced cracks developing along the axis of the longitudinal rebar and no transverse cracks being observed, indicating that the stirrups were not corroded (see Fig. 5).

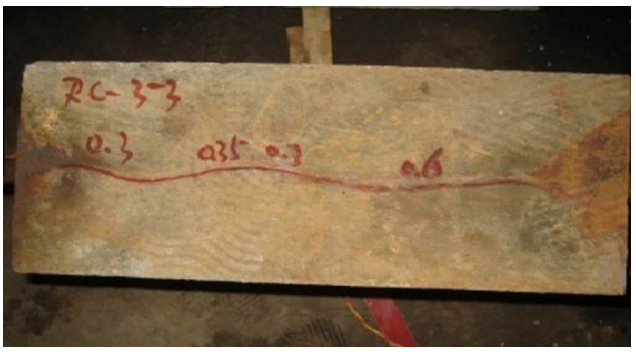


**Fig. 5.** Corrosion pattern of test beams.

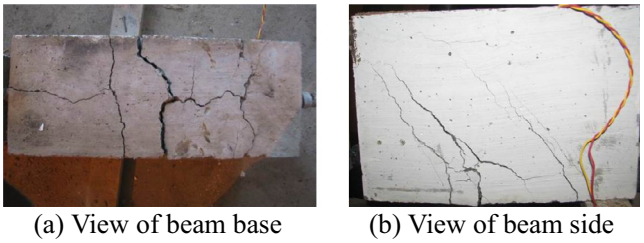


**Fig. 6.** Typical crack pattern of reinforced RAC beam.

A typical failure pattern after loading is shown in Fig. 6. For RAC beams containing non-corroded reinforcement, the first load-induced crack appeared at the base of each beam and formed across the longitudinal reinforcement, with cracking next developing vertically on the side of the beam (Fig. 6(a)) until these cracks intersected the level of the longitudinal rebar. The main diagonal crack was typically accompanied by 1–2 secondary oblique cracks (Fig. 6(b)). Following the development of the diagonal cracks on the side of the beam, cracking developed on the beam base oriented parallel to the direction of the longitudinal rebar. At this load level bar slip at the free end increased rapidly and the width of the inclined cracks further increased while the load value remained unchanged. The failure pattern of the RAC beam with corroded reinforcement was similar to that for the RAC beam containing non-corroded reinforcement such that there was little apparent effect due to the corrosion and RCA substitution. Significantly, although the test beam was composed of two symmetrical half-beams, because of material dispersion and fabrication error one of the half-beams developed damage before the other.

### 3.2. Characteristic values of bond-slip

As shown in Fig. 7, the magnitude of $T$ can be calculated according to Eq. (2):

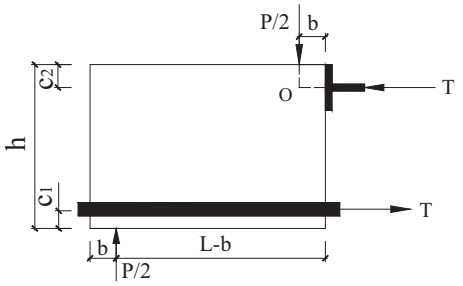


**Fig. 7.** Diagram for $T$ calculation.

**Table 3**
Bond-slip characteristic values.

| No. | η (%) | C (mm) | P (kN) | $P_0$ (kN) | τ (MPa) | *S* (mm) |
|---|---|---|---|---|---|---|
| RC1-0 | 0 | 0 | 120.0 | 87.6 | 8.99 | 2.50 |
| RC1-1 | 4.2 | 0.10 | 112.6 | 90.1 | 8.44 | 2.10 |
| RC1-2 | 6.0 | 0.35 | 95.1 | 77.9 | 7.13 | 1.03 |
| RC1-3 | 17.3 | 0.60 | 90.0 | 79.3 | 6.74 | 0.93 |
| RC2-0 | 0 | 0 | 106.0 | 88.0 | 7.94 | 1.54 |
| RC2-1 | 4.2 | 0.15 | 101.0 | 85.5 | 7.57 | 0.75 |
| RC2-2 | 6.0 | 0.35 | 88.2 | 82.1 | 6.60 | 0.19 |
| RC2-3 | 17.3 | 0.55 | 86.0 | 75.5 | 6.44 | 1.75 |
| RC3-0 | 0 | 0 | 101.0 | 70.9 | 7.56 | 1.25 |
| RC3-1 | 4.2 | 0.15 | 94.9 | 75.1 | 7.11 | 0.50 |
| RC3-2 | 6.0 | 0.35 | 94.1 | 76.6 | 7.05 | 1.07 |
| RC3-3 | 17.3 | 0.60 | 85.6 | 69.7 | 6.41 | 0.23 |

Where η is the theoretical corrosion rate, C is the maximum corrosion-induced crack width, P is the ultimate bearing capacity, $P_0$ is the load value when slip occurred at the free end of rebar, and *S* is slip at the free end.

$$T \times (h - c_1 - c_2) = \frac{P}{2} \times (L - 2b) \quad (2)$$

where $P$ is the applied load value; b is the distance between support and edge of beam ($b = 20$ mm); $T$ is the tension force on the longitudinal rebar; $c_1$ is the distance from rebar center to the base of beam ($c_1 = 45$ mm); and $c_2$ is the distance between steel web center and top of beam ($c_2 = 35$ mm). Substituting $b = 20$ mm, $c_1 = 45$ mm, $c_2 = 35$ mm, $h = 250$ mm and $L = 360$ mm into Eq. (2) produces: $T = 16P/17$. $T$ is then used to calculate the ultimate average bond strength ($\tau$) of reinforced RAC as follows:

$$\tau = T/(\pi d l_0) \quad (3)$$

where d is the diameter of rebar (d = 20 mm); $l_0$ is the embedment length of rebar ($l_0 = 200$ mm). Bond-slip characteristic values obtained from the beam tests are summarized in Table 3.

### 3.3. Influence of rebar corrosion and RCA replacement on bond-slip

The bond-slip curve for the right half-beam of RC1-1 is shown in Fig. 8, with the bond-slip curves for other tests being similar to that for RC1-1. It can be seen that the slip initially grew slowly with an increase of applied load, but increased suddenly once diagonal cracking had developed. The relationships for the ultimate average bond strength versus crack widths are drawn in Fig. 9, with Table 3 and Fig. 9 indicating that increased corrosion crack widths resulted in a rapid decrease of the ultimate average bond strength of RAC, and that the rate of decline reduced with an increase of RCA replacement.

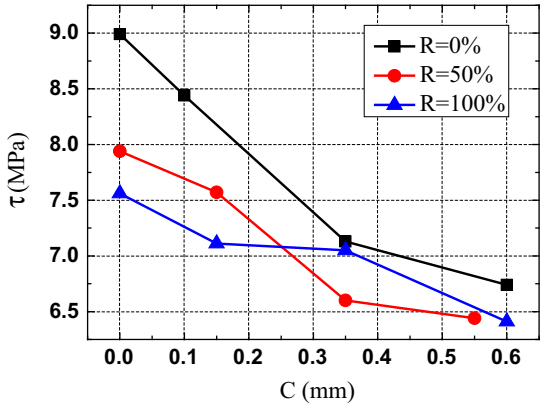


**Fig. 9.** τ-C relationship.

K is herein defined as $\tau_0/\tau$ to reveal the relative anti-sliding ability of a corroded reinforced RAC beam, where $\tau_0$ is the average bond strength when slip appears at a free end. Fig. 10 presents the relationship between K and C, which shows that the K value was in the range of 0.7–0.95 for concrete with different levels of RCA. In addition, with the increase of corrosion crack widths or corrosion rate, the K value first increased and then decreased. This trend is possibly attributable to the bursting force generated due to steel corrosion, resulting in an increase of the lateral restraining force imposed on the stirrups, which enhances the relative anti-sliding when the crack width or corrosion rate is relatively small, but once the crack widths increase above a certain value, the rela-

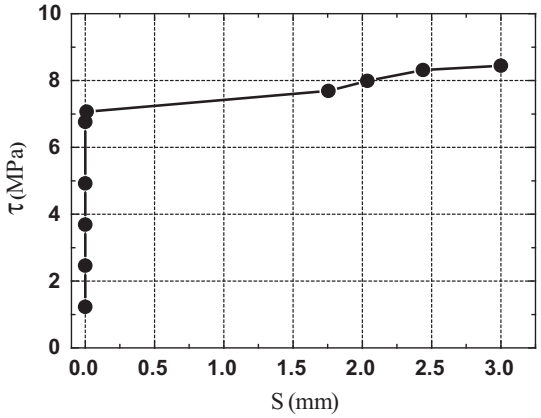


**Fig. 8.** Bond-slip curve of RC1-1.

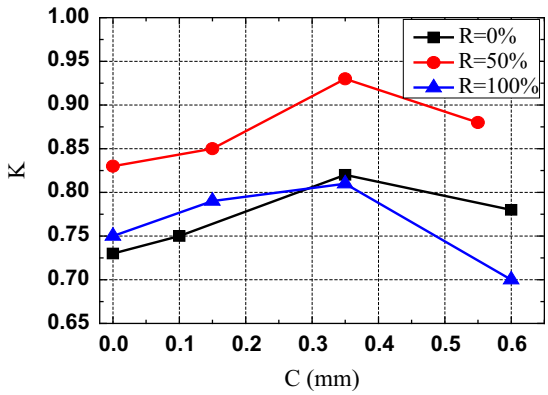


**Fig. 10.** K versus C.

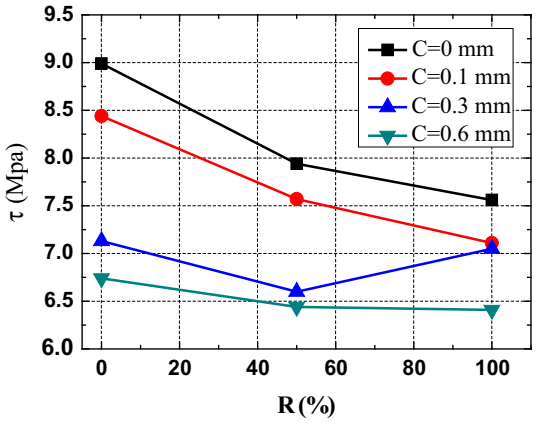


**Fig. 11.** τ versus R.

tive anti-sliding ability decreases because the confinement is exhausted.

The correlations between τ and replacement percentage are drawn in Fig. 11. It can be clearly observed that the ultimate bond strength generally decreased with an increase of replacement percentage, although RAC with 50% recycled coarse aggregate had a compressive strength that was equivalent to the values obtained for NAC. This observation can probably be explained by recognizing that there are more micro-cracks in the internal RCA and more weak aggregate boundaries in RAC, such that tensile cracking is most likely to occur at these weak boundaries when the RAC beam is subjected to bending and shearing stresses. Once a crack had initiated, it rapidly grew in both length and width until it had developed into a main diagonal crack which induced the observed decrease in ultimate bond strength.

### 3.4. Bond stress distribution of corroded reinforced RAC

The representative rebar strain distribution curves obtained from the tests are shown in Fig. 12. All curves show the characteristic that the strain value and the tangent slope gradually increase from the free end to the load end. Assuming that the bond stress distribution between adjacent strain gauges is uniform, one can calculate $\tau_j$ according to Eq. (4):

$$\tau_j = \frac{dT}{A} = \frac{A_s(\sigma_{i+1} - \sigma_i)}{\pi d h_i} = \frac{E_s A_s(\varepsilon_{i+1} - \varepsilon_i)}{\pi d h_i} \quad (4)$$

where $\tau_j$ is the uniform bond stress between adjacent gauges; $dT$ is the difference between the tension forces at the two ends of each micro segment; $\sigma_i$, $\sigma_{i+1}$ and $\varepsilon_i$, $\varepsilon_{i+1}$ are the tension stresses and the measured rebar strains at the (i) and (i+1) gauge points separately; $h_i$ is the distance between adjacent gauges; and $E_s$, $A_s$ and $d$ are the elastic modulus, the sectional area and the rebar diameter respectively.

By numerically integrating the bond stress distribution along the anchorage length according to Eq. (5), the theoretical tension force $P$ should equal the tension force $T$ calculated by Eq. (2). If the two values are found to be unequal then the difference between these values should be deducted from each micro segment according to the proportion of $h_i$ to make a fine modification. At the conclusion of this process a series of smooth bond

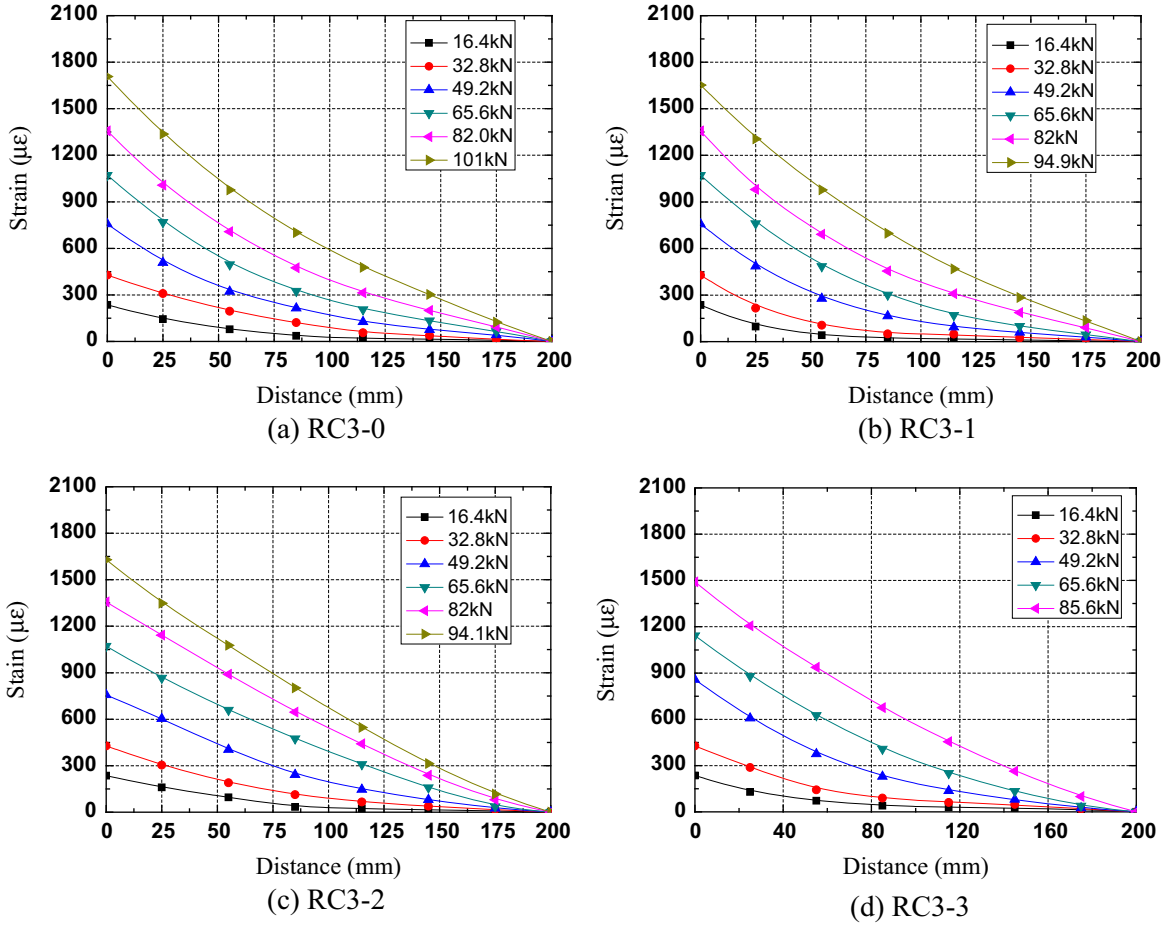


**Fig. 12.** Representative rebar strain distribution along the anchorage length.

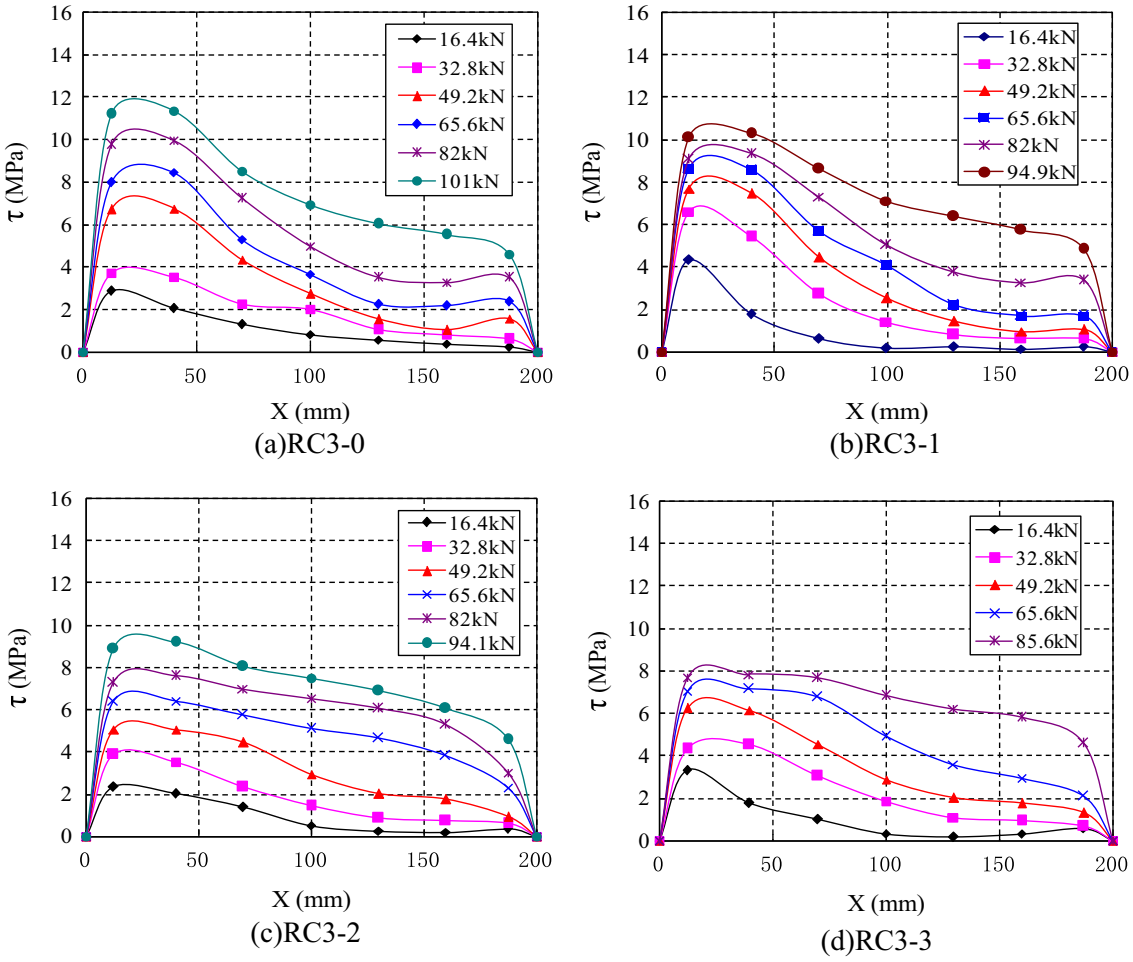


**Fig. 13.** Representative bond stress distribution curves.

stress distribution curves for various loading conditions were drawn as shown in Fig. 13.

$$P = \sum_{j=1}^{n} (\tau_j \cdot \pi d h_i) \tag{5}$$

From Fig. 13 it can be seen that the bond stress distribution curves of the reinforced concrete beams with different levels of RCA substitution and different crack widths were similar. For low levels of applied loading the bond stress near the load end increased rapidly, with the bond stress then being gradually transferred to the free end with increasing load increments. It was found that only the ultimate bond strength decreased with an increase of RAC crack widths, whereas the regularity of the bond stress distribution remained unchanged due to the stirrup confinement. Additionally, Fig. 13 reveals that the bond stress value in the vicinity of the load end (X = 12.5 mm) was always greater than the corresponding stress near the free end (X = 187.5 mm), which was unaffected by the crack widths and RCA substitution. This result is similar to that reported by Kankam and Zhang [22,35], but differs from the test results obtained by Zhao [30], who found that the middle of the RAC specimens exhibited the highest bond rigidity when using a pull-out test.

### 3.5. Bond position function

To analyze the bond position function of RAC beams, the bond stress distribution curves were normalized by plotting the relative location $X/l_0$ as the X-axis and plotting the relative bond stress ($\psi = \tau_j/\tau$) as the Y-axis. The relationship of $\psi$ and $X/l_0$ reflects the bond rigidity distribution at different locations. Fig. 14 shows the comparison of bond rigidity distribution curves of RAC beams with different crack widths and different RCA replacement percentages for data obtained at ultimate loading. It was found that the bond rigidity increased sharply at both ends and almost linear decreased in the range of 0.15–0.85 times the anchorage length. In addition, the bond rigidity became more uniform as the crack widths increased, whilst increasing RCA substitution had little effect on the bond rigidity curves.

It was observed that the bond rigidity curves exhibited characteristics that approached straight lines at both ends whilst linearly decreasing in the middle segment (Fig. 14). Therefore, for practical engineering application a trilinear model was established for the bond position function as shown in Fig. 15(a), where four control points define this model: 1 (0, 0), 2 (0.15, $A_1$), 3 (0.85, $A_2$), and 4 (1, 0). $A_1$ and $A_2$ can be determined by numerical fitting:

(1) C = 0 mm: $A_1 = 1.49$, $A_2 = 0.67$.
(2) C ≈ 0.15 mm: $A_1 = 1.42$, $A_2 = 0.71$.
(3) C ≈ 0.35 mm: $A_1 = 1.3$, $A_2 = 0.82$.
(4) C ≈ 0.6 mm: $A_1 = 1.21$, $A_2 = 0.9$.

The results demonstrate that the value of $A_1$ decreases whereas the value of $A_2$ increases with crack width increment which can be also obviously observed from Fig. 15(b). This observation demonstrates that the corrosion or crack width affects the bond position,

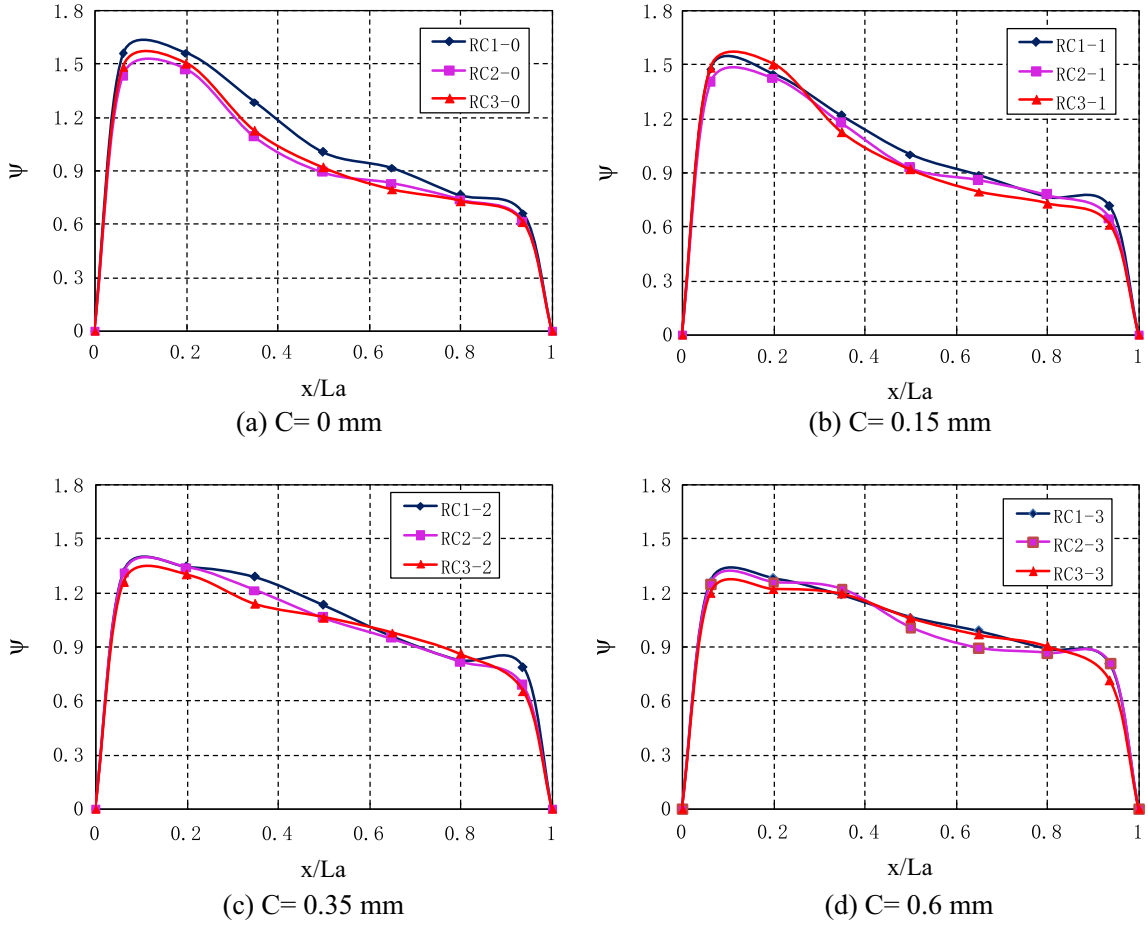


**Fig. 14.** Bond rigidity curves for different crack widths.

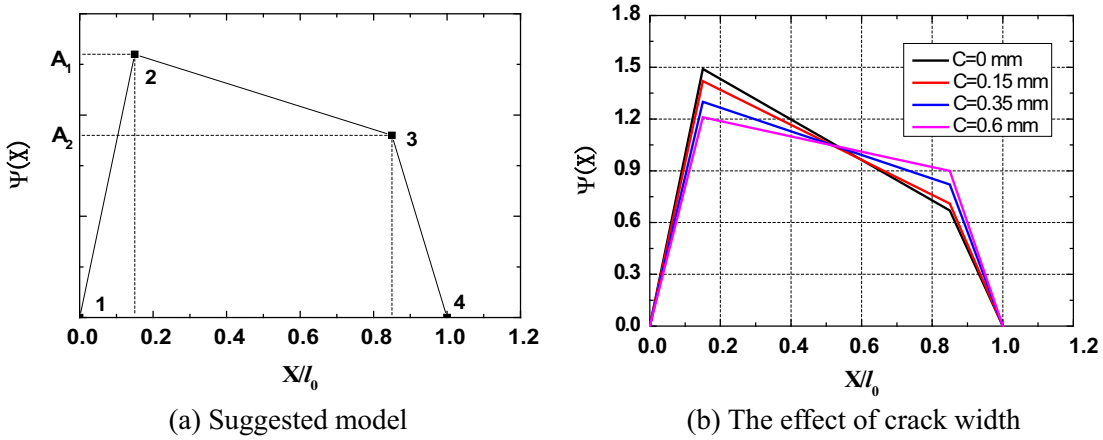


**Fig. 15.** Bond position function model.

and the bond rigidity distribution became more uniform as the crack widths increased. Once C > 0.6 mm, it can be inferred that $A_1 = A_2 = 1.0$, id est, the bond stress distribution is uniform over the anchorage length.

## 4. Conclusions

Twelve beam tests were conducted to determine the influence of RCA substitution and crack widths on bond strength and to establish bond rigidity curves for reinforced RAC. The main conclusions from this study were as following:

(1) The ultimate average bond strength ($\tau$) of reinforced RAC beams decreases overall with an increase of RCA replacement percentage and corrosion crack widths. With an increase of RCA substitution for RC1-2, RC2-2 and RC3-2 the ultimate average bond stress $\tau$ declined at rates of 20.7%, 16.8% and 6.8%, which demonstrates that the rate of decline reduced with an increase of RCA substitutuion.

(2) As corrosion rate increases, the relative anti-sliding ability (K) of reinforced RAC beams first increases and then deceases, and the maximum K value appears as C = 0.35 mm for different levels of RCA substitution.
(3) The bond rigidity curves for reinforced RAC beams are similar to that of NAC beams, with a sharp increase of bond rigidity at both anchorage ends, and a linear decrease of bond rigidity in the range of 0.15–0.85 times the anchorage length. This observation supplements Zhao's finding, which only indicate the middle of the specimens exhibited the highest bond rigidity. In addition, RCA substitution has little effect on bond rigidity.
(4) A trilinear model is suggested to establish the bond position function of RAC beams containing corroded reinforcement. With an increase of corrosion rate or crack width, the value of parameter $A_1$ in this model decreases whereas the value of parameter $A_2$ increases. Bond strength can be deemed as uniform over the anchorage length when the crack width greater than 0.6 mm.

## Acknowledgments

This study was supported by funding received from the Natural Science Foundation of China (Nos. 51308135 and 51478126) and the program of Guangxi Natural Science Foundation (No. 2014GXNSFBA118242).

## References

[1] B. Yin, Study on Management Policy of Building Demolition (In Chinese), Chinese academy of building research, Beijing, 2014.
[2] M. Behera, S.K. Bhattacharyya, A.K. Minocha, R. Deoliya, S. Maiti, Recycled aggregate from C&D waste & its use in concrete – A breakthrough towards sustainability in construction sector: A review, Constr Build Mater 68 (2014) 501–516.
[3] S.M. Levy, P. Helene, Durability of recycled aggregates concrete: a safe way to sustainable development, Cem Concr Res 34 (11) (2004) 1975–1980.
[4] M.C. Limbachiya, T. Leelawat, R.K. Dhir, Use of recycled concrete aggregate in high-strength concrete, Mater Struct 33 (2000) 574–580.
[5] K. Yoda, A. Shintani, Building application of recycled aggregate concrete for upper-ground structural elements, Constr Build Mater 67 (2014) 379–385.
[6] M. Etxeberria, Marı' AR, and Va'zquez E. Recycled aggregate concrete as structural material, Mater Struct 40 (5) (2007) 529–541.
[7] W. Choi, H. Yun, S. Kim, Flexural performance of reinforced recycled aggregate concrete beams, Mag Concr Res 64 (9) (2012) 837–848.
[8] I.S. Ignjatović, S.B. Marinković, Z.M. Mišković, A.R. Savić, Flexural behavior of reinforced recycled aggregate concrete beams under short-term loading, Mater Struct 46 (6) (2012) 1045–1059.
[9] T.H.-K. Kang, W. Kim, Y.-K. Kwak, S.-G. Hong, Flexural testing of reinforced concrete beams with recycled concrete aggregates, ACI Struct. J. 111 (3) (2014) 607–616.
[10] M. Breccolotti, A.L. Materazzi, Structural reliability of eccentrically-loaded sections in RC columns made of recycled aggregate concrete, Eng Struct 32 (11) (2010) 3704–3712.
[11] W.-C. Choi, H.-D. Yun, Compressive behavior of reinforced concrete columns with recycled aggregate under uniaxial loading, Eng Struct 41 (2012) 285–293.
[12] J. Xiao, X. Huang, L. Shen, Seismic behavior of semi-precast column with recycled aggregate concrete, Constr Build Mater 35 (2012) 988–1001.
[13] V.C.L. Gonzalez, G. Moriconi, The influence of recycled concrete aggregates on the behavior of beam–column joints under cyclic loading, Eng Struct 60 (2014) 148–154.
[14] V. Corinaldesi, G. Moriconi, Behavior of Beam-Column Joints Made of Sustainable Concrete under Cyclic Loading, J Mater Civ Eng 18 (2006) 650–658.
[15] X. Li, Recycling and reuse of waste concrete in China Part II. Structural behaviour of recycled aggregate concrete and engineering applications, Resour Conserv Recy 53 (3) (2009) 107–112.
[16] J. Xiao, H. Falkner, Bond behaviour between recycled aggregate concrete and steel rebars, Constr Build Mater 21 (2) (2007) 395–401.
[17] M. Guerra, F. Ceia, J.D. Brito, E. Júlio, Anchorage of steel rebars to recycled aggregates concrete, Constr Build Mater 72 (2014) 113–123.
[18] M.J.R. Prince, B. Singh, Bond behaviour between recycled aggregate concrete and deformed steel bars, Mater Struct 47 (3) (2013) 503–516.
[19] L. Butler, J.S. West, S.L. Tighe, The effect of recycled concrete aggregate properties on the bond strength between RCA concrete and steel reinforcement, Cem Concr Res 41 (10) (2011) 1037–1049.
[20] G. Fathifazl, A.G. RazaqpurIsgor, O.B. Isgor, A. Abbas, B. Fournier, S. Foo, Bond performance of deformed steel bars in concrete produced with coarse recycled concrete aggregate, Can J Civil Eng 39 (2) (2012) 128–139.
[21] ASTM A944-10. Standard test method for comparing bond strength of steel reinforcing bars to concrete using beam-end specimens, Annual Book of ASTM Standard, 2010.
[22] C.K. Kankam, Relationship of Bond Stress, Steel Stress, and Slip in Reinforced Concrete, J Struct Eng 123 (1) (1997) 79–85.
[23] S. Wang, J. Huang, J. Zhang, D. Pan, An Investigat ion on Concrete Corrosion of Seaport Wharf in South China and Analysis of Structures'Durability (In Chinese), Port Water Eng 317 (6) (2000) 8–12.
[24] J. Dong, E. Han, W. Ke, Introduction to atmospheric corrosion research in China, Sci Technol Adv Mater 8 (7–8) (2007) 559–565.
[25] L. Peng, M.G. Stewart, Climate change and corrosion damage risks for reinforced concrete infrastructure in China, Struct Infrastruct Eng (2014) 1–18.
[26] Y. Auyeung, P. Balaguru, L. Chung, Bond behavior of corroded reinforcement bars, ACI Mater J 97 (2) (2000) 214–220.
[27] K. Bhargava, A.K. Ghosh, Y. Mori, S. Ramanujam, Corrosion-induced bond strength degradation in reinforced concrete-Analytical and empirical models, Nucl Eng Des 237 (11) (2007) 1140–1157.
[28] D. Coronelli, Corrosion cracking and bond strength modeling for corroded bars in reinforced concrete, ACI Struct J 99 (3) (2002) 267–276.
[29] C. Fang, K. Lundgren, M. Plos, K. Gylltoft, Bond behaviour of corroded reinforcing steel bars in concrete, Cem Concr Res 36 (10) (2006) 1931–1938.
[30] Y. Zhao, H. Lin, K. Wu, W. Jin, Bond behaviour of normal/recycled concrete and corroded steel bars, Constr Build Mater 48 (2013) 348–359.
[31] Chinese standard GB/T25177-2010. Recycled Coarse Aggregate for Concrete, 2010, p. 2–3.
[32] Chinese standard GB 175–2007. Common Portland Cement, 2007, p. 2–16.
[33] C.S. Poon, Z.H. Shui, L. Lam, Effect of microstructure of ITZ on compressive strength of concrete prepared with recycled aggregates, Constr Build Mater 18 (6) (2004) 461–468.
[34] G. Mancini, F. Tondolo, Effect of bond degradation due to corrosion - a literature survey, Struct Concr 15 (3) (2014) 408–418.
[35] W. Zhang, Y. Zhao, Bond-slip relationship between corroded steel bars and concrete (In Chinese), China Civ Eng 34 (5) (2001) 40–44.